ACS APPLIED MATERIALS & INTERFACES

RESEARCH ARTICLE

www.acsami.org

Adsorption of Lead(II) on O_2-Plasma-Oxidized Multiwalled Carbon Nanotubes: Thermodynamics, Kinetics, and Desorption

Xin-Yao Yu, Tao Luo, Yong-Xing Zhang, Yong Jia, Bang-Jing Zhu, Xu-Cheng Fu, Jin-Huai Liu,* and Xing-Jiu Huang*

Research Center for Biomimetic Functional Materials and Sensing Devices, Institute of Intelligent Machines, Chinese Academy of Sciences, Hefei, Anhui 230031, People's Republic of China

Supporting Information

ABSTRACT: O_2-plasma-oxidized multiwalled carbon nanotubes (po-MWCNTs) have been used as an adsorbent for adsorption of lead(II) in water. Scanning electron microscopy, transmission electron microscopy, X-ray diffraction, and Raman spectroscopy measurements show that the bulk properties of MWCNTs were not changed after O_2-plasma oxidation. The adsorption capacity of MWCNTs for lead(II) was greatly enhanced after plasma oxidation mainly because of the introduction of oxygen-containing functional groups onto the surface of MWCNTs. The removal of lead(II) by po-MWCNTs occurs rather quickly, and the adsorption kinetics can be well described by the pseudo-second-order model. The adsorption isotherm of lead(II) onto MWCNTs fits the Langmuir isotherm model. The adsorption of lead(II) onto MWCNTs is strongly dependent upon the pH values. X-ray photoelectron spectroscopy analysis shows that the adsorption mechanism is mainly due to the chemical interaction between lead(II) and the surface functional groups of po-MWCNTs. The thermodynamic parameters ($\Delta H°$, $\Delta S°$, and $\Delta G°$) calculated from the adsorption isotherms suggest that the adsorption of lead(II) onto MWCNTs is endothermic and spontaneous. The regeneration performance shows that lead(II) can be easily regenerated from po-MWCNTs by altering the pH values of the solution.

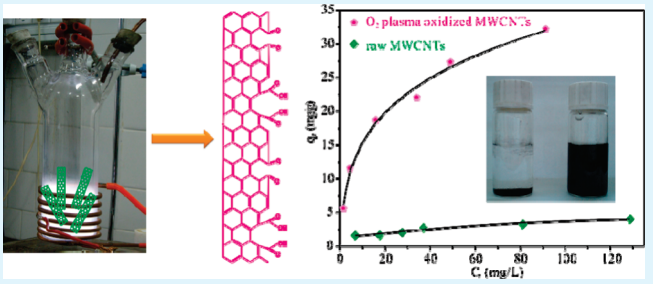

KEYWORDS: multiwalled carbon nanotubes, O_2 plasma, adsorption, lead(II), thermodynamics, kinetics, desorption

1. INTRODUCTION

Recently, increasing interest has been focused on the removal of heavy-metal ions from drinking water because of their toxicity to our health. Among all of the heavy-metal ions, lead has been identified as one of the most toxic heavy metals because of its detrimental effects on the human nervous system, blood circulation system, kidneys, and reproductive system.[1,2] Adsorption has been recognized as a promising technology for the purification of water with trace levels of heavy-metal ions because of its advantages of cost-effectiveness, simple operation and environmental friendliness.

Carbon nanotubes (CNTs) with outer diameters in the range of 1−100 nm have attracted special interest in multidisciplinary studies and have shown promising applications. Because of their relatively large specific area and hollow and layered structures, CNTs have been used as adsorption materials for the removal of organic and inorganic contaminants.[1,3−15] However, one of the major obstacles for the development of CNT-based adsorbents is their insolubility and fewer surface functional groups. At present, the chemical modification methods are most common. In these processes, CNTs are normally refluxed or sonicated in a strong acid, such as HNO_3 and/or H_2SO_4, to introduce oxygen-containing functional groups, such as −C═O, −C−OH, and −COOH, to their surfaces. CNTs oxidized by strong acid have been reported for the removal of Pb^{2+} in water.[1,11−15] However, the harsh conditions of inherent strong acid may introduce wall damage, decreasing their stability and even cleaving them into shorter pieces.[16,17] Especially, these wet chemical modification processes themselves are not environmentally friendly or time-consuming.

In recent years, plasma surface functionalization has gained lots of attention because it is a solvent-free, time-efficient, versatile, and environmentally friendly procedure for surface modification. The plasma technique has been shown to be effective in the facial modification of CNTs.[16,18−20] We have used the plasma-functionalized multiwalled CNTs (MWCNTs) as a substrate for the deposition of platinum nanoparticles.[17] It has been shown that plasma surface modification treatment does not cause a large amount of structural damage to the MWCNTs.[17]

Recently, Charlier et al.[21] and Zanolli et al.[22] have used O_2-plasma-treated MWCNTs for gas-sensing applications. However, to the best of our knowledge, the application of O_2-plasma-oxidized MWCNTs in the removal of heavy-metal ions from solutions is not

Received: April 6, 2011
Accepted: June 15, 2011
Published: June 15, 2011

available. In this study, MWCNTs were oxidized by O_2 plasma to increase the oxygen-containing functional groups on their surfaces, thus improving the adsorption performance for lead(II) in water. The effects of the plasma oxidation time, contact time, and temperature on the adsorption of lead(II) onto O_2-plasma-oxidized MWCNTs were studied. In the adsorption kinetics study, the adsorptions of lead(II) by raw-MWCNTs, O_2-plasma-oxidized MWCNTs, and coconut shell activated carbon (AC) were compared. The effects of the pH value on the adsorption/desorption of lead(II) onto/from MWCNTs were also studied. The main possible mechanisms of O_2-plasma oxidation and adsorption of lead(II) onto O_2-plasma-oxidized MWCNTs were proposed.

2. EXPERIMENTAL SECTION

Chemicals. All chemicals used in this study were of analytical grade. Stock solutions of 1000 mg/L lead(II) were prepared from $Pb(NO_3)_2$ in deionized water. The stock solution was further diluted with deionized water to the required lead(II) concentrations in the adsorption experiments. Adjustment of the pH was undertaken using 0.1 M HNO_3 and 0.1 M NaOH. Coconut shell AC with a diameter of 20−40 mesh was purchased from Hefei Chenming Activated Carbon Corp. (Hefei, China). Deionized water was used throughout the work. MWCNTs were obtained from Chengdu Institute of Organic Chemistry of the Chinese Academy of Sciences. The MWCNTs are assigned to raw-MWCNTs. The purity of the raw-MWCNTs is about 95%, with a 0.23% and 0.93% content of iron and nickel catalysts, respectively. The amorphous carbon content is about 4%.

O_2-Plasma Oxidation of MWCNTs. The apparatus for O_2-plasma oxidation was depicted in our previous paper.[17] A plasma generator induced by a radio-frequency inductively coupled plasma was used in this study. Prior to ignition of the O_2 plasma, the pressure in the reactor was evacuated to 2.0 Pa. Pure O_2 gas was then introduced into the reactor via a needle valve. Plasma ignition occurred at 5 Pa with a frequency of 13.56 MHz and a supplied power of 50 W. MWCNTs were oxidized by O_2 plasma for different times (3, 10, and 30 min) under continuous stirring. The O_2-plasma-oxidized MWCNTs are assigned to po-MWCNTs.

Adsorption and Regeneration Experiments. Adsorption kinetics was carried out to achieve the equilibrium time. In adsorption kinetics study, raw-MWCNTs and po-MWCNTs were compared with coconut shell AC. Experiments were carried out at 293 K using a 500 mL conical flask containing 300 mg of adsorbents and 200 mL of a lead(II) solution with an initial concentration of 9 or 17 mg/L at pH = 5.0. The conical flasks were sealed with glass stoppers, and these samples were placed on a shaker for stirring. At predetermined time intervals, stirring was interrupted while 4 mL of supernatant solutions were pipetted from the conical flask, and samples were filtered using 0.45 μm membrane filters. The final lead(II) concentrations remaining in the solution were analyzed.

The other adsorption experiments were conducted in polyethylene centrifuge tubes by using the batch technique. The pH values were adjusted with a negligible amount of 0.1 M HNO_3 or NaOH. Except when the pH effect was studied, all adsorption experiments were carried out at an initial pH of 5.0.

The adsorption capacity of the adsorbents for lead(II) was calculated according to the following equation:

$$q_e = \frac{(C_0 - C_e)V}{m} \quad (1)$$

where C_0 and C_e represent the initial and equilibrium metal ion concentrations (mg/L), respectively. V is the volume of the metal ion solution (mL), and m is the amount of adsorbent (mg).

To evaluate the regeneration capacity, po-MWCNTs of adsorption equilibrium at an initial lead(II) concentration of 134 mg/L were dried at 353 K for 6 h and then were dispersed into deionized water with different pH values (from 2 to 5.5). These samples were mounted on the shaker for 3 h of stirring. The lead(II) concentrations were remeasured, and the regeneration results were then obtained. These adsorption/desorption processes were repeated three times to ascertain the desorption capability of po-MWCNTs.

All of the experimental data were the averages of triplicate determinations. The relative errors of the data were about 5%.

Characterization. The scanning electron microscopy images were taken by using a field-emission scanning electron microscope (JEOL JSM-6700F, 10 kV). The transmission electron microscopy (TEM) investigations were carried out on a JEOL JEM-2000EX microscope operating at 100 keV. X-ray diffraction (XRD) was performed on a D/MaxIIIA X-ray diffractometer (Rigaku Co., Japan), using Cu Kα ($\lambda_{K\alpha_1}$ = 1.5418 Å) as the radiation source. Nitrogen adsorption has been used to characterize MWCNTs and oxidized MWCNTs used in the adsorption of heavy-metal ions.[11,12] The specific surface area and pore-size distribution (PSD), which have some effects on heavy-metal adsorption, can be obtained using nitrogen adsorption. It has been demonstrated that physical adsorption, which is dependent on the specific surface area, is not the main adsorption mechanism for heavy-metal-ion adsorption onto the oxidized MWCNTs.[12] The nitrogen adsorption and desorption isotherms at 77 K were measured with a Micromeritics ASAP 2020 M analyzer. The Brunauer−Emmett−Teller (BET) equation was used to obtain the specific surface areas and adsorption average pore widths (W_p). For MWCNTs, the pores are those inner cavities in the mesopore range and aggregated pores. The amount of nitrogen adsorbed at relative pressures near unity (P/P_0 = 0.99) was employed to determine the total pore volume (V_t). The t-plot theory was used to calculate the micropore surface area (S_{mi}), external surface area (S_e), and micropore volume (V_{mi}). The t-plot method is attributed to Lippens and de Boer.[23] They proposed the plotting of the nitrogen-adsorbed volume (V_a) at different P/P_0 values as a function of the layer thickness (t). Microporous solids yield linear plots that intercept the V_a ordinate at a finite value at t = 0 (P/P_0 = 0). This linear plot can be used to calculate the external surface area of the solid, and the slope of the line drawn from the origin to the monolayer point can be used to calculate the surface area of the micropores and the external surface. Density functional theory (DFT) was employed to analyze the successive PSD curves. DFT provides a microscopic treatment of sorption phenomena in micro- and mesopores on a molecular level, i.e., based on statistical mechanics. Complex mathematical modeling of gas−solid and gas−gas (gas−liquid) interactions plus geometrical considerations (pore geometry) leads to realistic density profiles for the confined fluid as a function of the temperature and pressure. From these density profiles, the amount adsorbed can be derived. Gas−solid interactions are calibrated against real isotherm data of nonporous material, and gas−gas−liquid interactions are calibrated against physical data, e.g., boiling points. For pore-size analysis, a kernel is created that consists of up to 100 theoretical, individual pore isotherms.[24] Electron spin resonance (ESR) spectra were recorded by a JES-RE1X (JEOL) spectrometer with X-band and 100 kHz field modulation. Raman spectroscopy was carried out on a Lab Ram HR Raman spectrometer excited at 514.5 nm by an argon-ion laser. X-ray photoelectron spectroscopy (XPS) analyses of the samples were conducted on a VG ESCALAB MKII spectrometer using an Mg Kα X-ray source (1253.6 eV, 120 W) at a constant analyzer. The energy scale was internally calibrated by referencing the binding energy (E_b) of the C 1s peak at 284.60 eV for contaminated carbon. The metal concentration was determined in the liquid phase using an inductively coupled plasma atomic emission spectrometer (Jarrell-Ash model ICAP 9000).

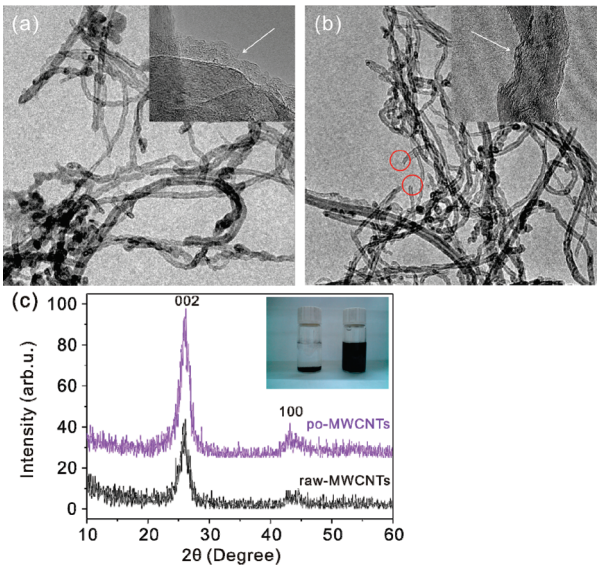

Figure 1. TEM images of (a) raw-MWCNTs and (b) po-MWCNTs after oxidation for 30 min. (c) XRD patterns of raw-MWCNTs and po-MWCNTs. The insets of parts a and b show the high-resolution TEM images of raw-MWCNTs and po-MWCNTs, and the inset of part c shows a comparison of the dispersion properties of raw-MWCNTs (left) and po-MWCNTs (right) in deionized water after settling for 20 h. Unless otherwise stated, po-MWCNTs were designated as MWCNTs oxidized by plasma for 30 min.

3. RESULTS AND DISCUSSION

Characterization. Parts a and b of Figure 1 show the TEM images of the raw-MWCNTs and typical O_2-plasma-oxidized MWCNTs, respectively. It is seen that both raw-MWCNTs and po-MWCNTs have an outer diameter of 10−30 nm. TEM images confirm that the microstructures and the diameter distribution of the nanotubes were without obvious change after the O_2-plasma oxidation. This indicates that the ion bombardment of the O_2-plasma treatment in this study is moderate. From Figure 1a,b, we can see that before plasma treatment the caps of MWCNTs are not open, while after plasma treatment, the caps of MWCNTs are partially opened (see the red circles in Figure 1b). Additionally, high-resolution TEM (the insets in Figure 1a,b) was used to observe the detailed structural information of raw-MWCNTs and po-MWCNTs. From the inset of Figure 1a, we can see that there are some disordered or amorphous carbon layers outside the nanotubes, as indicated by the white arrow. After O_2-plasma oxidation, the amorphous carbon layer was removed and the multilayer structure of MWCNTs remains intact although there were some defects on the outermost walls, as indicated by the white arrow, which can be seen from the inset of Figure 1b. Figure 1c shows the XRD patterns of the raw-MWCNTs and typical O_2-plasma-oxidized MWCNTs. The most intense peaks of MWCNTs correspond to the (002) and (100) reflections.[14] Because the ratio of peak 100 to peak 002 (I_{100}/I_{002}) is dependent on the planar order of CNTs,[25] the changes of the values of I_{100}/I_{002} were investigated. The results show that I_{100}/I_{002} of the two samples are both close to 0.3, suggesting that the po-MWCNTs still have the same cylinder wall structure as the raw-MWCNTs, and the interplanar spacing of CNTs remains the same after O_2-plasma oxidation. In addition, the formation of oxygen-containing functional groups during plasma oxidation and their interaction with water caused the nanotubes to produce stable suspensions. No aggregation appeared to occur in the suspension of po-MWCNTs even after 20 h of settling time (the inset in Figure 1c).

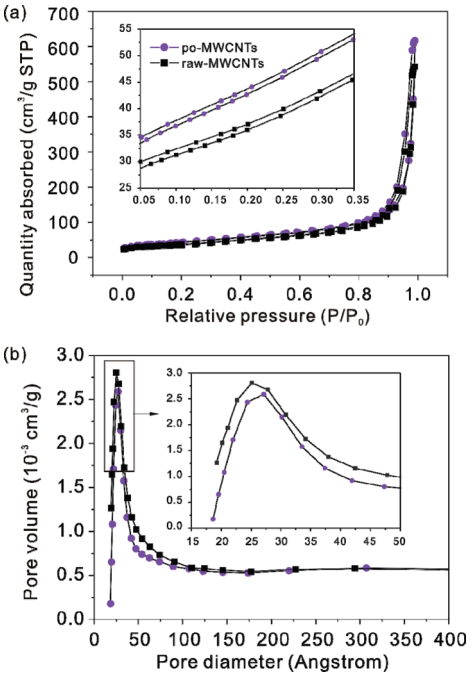

Figure 2. (a) BET nitrogen adsorption isotherms and (b) PSDs of raw-MWCNTs and po-MWCNTs.

Figure 2a shows the nitrogen adsorption isotherms measured at 77 K for the raw-MWCNTs and po-MWCNTs. The inset of Figure 2a was the magnified part ($0.05 < P/P_0 < 0.35$) of the isotherms. The PSDs of raw-MWCNTs and po-MWCNTs are shown in Figure 2b. It can be seen that the pores of both raw-MWCNTs and po-MWCNTs are in the micropore range (the inset in Figure 2b). Table S1 in the Supporting Information shows the changes in the microstructural properties of the MWCNTs such as the specific surface area and microspore volume. It is found that, compared with the raw-MWCNTs, the specific surface area of the po-MWCNTs increased by 19.68% and the micropore volume and the average pore diameter decreased after O_2-plasma oxidation. All of these may be due to the removal of impurities, the partial opening of some caps of MWCNTs, and the increase of functional groups and surface defects on the surface of MWCNTs introduced by O_2-plasma oxidation.

The change of the ESR spectra of MWCNTs after O_2-plasma oxidation is shown in Figure 3a. It is apparent that the spectral intensity increases after plasma oxidation. As the plasma oxidation time increases, the peak intensity increases. This augmentation is related to the increase in unpaired electrons and free radicals created on the surface of MWCNTs after plasma oxidation.[26,27] Figure 3b shows the Raman spectra of MWCNTs before and after O_2 oxidation as a function of the oxidation time. In the Raman spectra, the G band of MWCNTs is close to the highly oriented pyrolytic graphite, which exhibits a single peak at approximately 1578 cm^{-1} related to the E_{2g} tangential mode, and the D band of MWCNTs exhibits a single peak at approximately 1351 cm^{-1} related to the disorder-induced feature.[28] The ratio of the D-band intensity (I_D) to the G-band intensity (I_G) represents

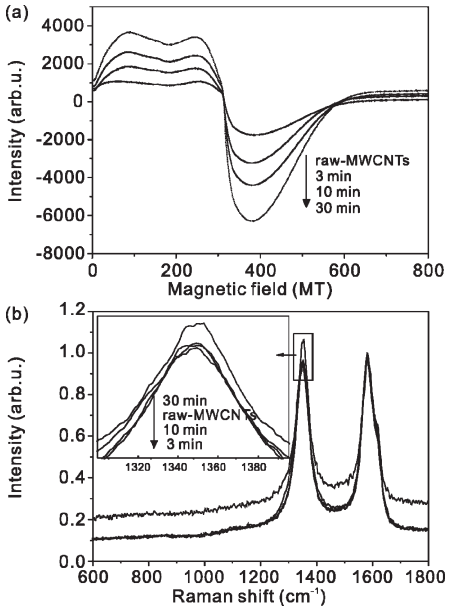

Figure 3. (a) ESR spectra and (b) Raman spectra of po-MWCNTs with different oxidation times.

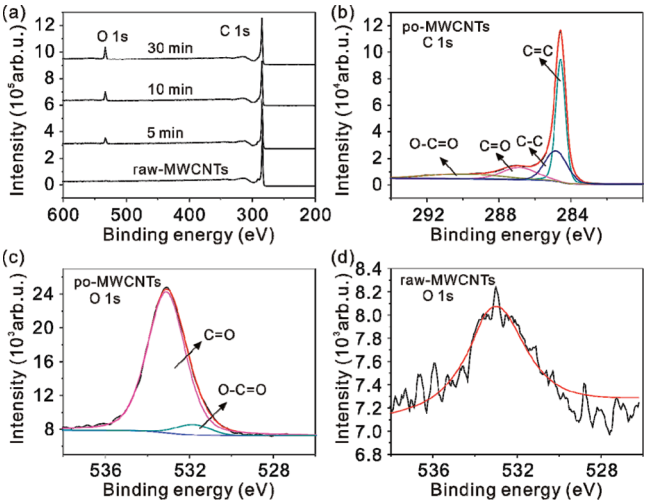

Figure 4. (a) XPS wide scan of po-MWCNTs with different oxidation times. (b–d) High-resolution C 1s and O 1s spectra of po-MWCNTs, respectively. (d) High-resolution O 1s spectrum of raw-MWCNTs.

the disorder level of MWCNTs.[28] The smaller ratio of I_D/I_G indicates that the MWCNTs possess fewer defects in the carbon structure or reduced amorphous carbons remaining on the surface of the MWCNTs. The I_D/I_G ratios of MWCNTs oxidized by O_2 plasma at different oxidation times are shown in Table S2 in the Supporting Information. It can be seen that the ratio of I_D/I_G decreased from 0.9774 to 0.9471 after 3 min of oxidation and then increased to 1.0895 after 30 min of oxidation. This may be the result of the removal of some amorphous carbon materials and other impurities after 3 min of oxidation.[29] Further oxidation may introduce some defects on the surface of the nanotubes, which is consistent with TEM studies.[30]

XPS is usually considered to be a powerful technique for identifying groups attached to the surface of MWCNTs. In Figure 4a, the XPS survey spectra reveal the presence of carbon and oxygen on the raw-MWCNTs and po-MWCNTs, and the oxygen atomic percentage can reach from 0.94% to 11.57% when oxidized by plasma for 30 min (Figure 4c,d). This indicates that the oxygen-containing functional groups were effectively grafted onto MWCNTs by O_2-plasma oxidation.[18,25,30] The C 1s spectrum (Figure 4b) of po-MWCNTs can be deconvoluted into four Gaussian peaks centered at 284.5 ± 0.2, 285.0 ± 0.2, 286.6 ± 0.2, and 289.9 ± 0.2 eV.[20,30] Here, the main peak at about 284.5 eV originates from the graphitelike sp^2 carbon, which indicates the graphite level. The peak at about 285.0 eV is assigned to the diamondlike sp^3 carbon, which indicates the disorder level. The peaks at about 286.6 and 289.9 eV correspond to carbonyl (or ether) and carboxyl (or ester) signals, respectively. The O 1s spectrum (Figure 4c) of po-MWCNTs peaks were deconvoluted into two Gaussian peaks: the peak at 531.8 ± 0.2 eV and the peak at 533.2 ± 0.2 corresponding to C═O and O—C═O species,[31] respectively. The results of O 1s are consistent with those of C 1s. Table S2 in the Supporting Information summarizes the atomic percentages of carbon and oxygen, different chemical states of C 1s and its relative percentage, and the oxygen atom percentage after XPS peak fitting and quantitative analysis.

From Table S2 in the Supporting Information, we can see that the relative percentages of sp^2 and sp^3 carbon decreased after O_2-plasma oxidation, suggesting that there is an increase in the average number of bonds between carbon and oxygen.[25] In addition, as shown in Table S2 in the Supporting Information, the relative percentage of oxygen increased when the plasma oxidation time increased. The fractions of both carbonyl (C═O) and carboxyl (−COOH) functional groups increased with an increase in the plasma oxidation time. Moreover, these oxygen-containing functional groups caused a rise in the negative charge on the carbon surface, and the oxygen atoms in the functional groups donate a single pair of electrons to metal ions, which consequently increased their cation-exchange capacity.[32]

On the basis of the above analysis, a possible mechanism for O_2-plasma oxidation of MWCNTs was proposed. The proposed O_2-plasma-oxidation mechanism of MWCNTs is shown in Figure S1 in the Supporting Information. First, some of the caps, which are the most reactive parts of MWCNTs, are opened, and the amorphous carbon layer is removed. Second, the unsaturated bonds of sp^2 C═C in CNTs are most active and susceptible to plasma attack.[33] Because of dissociation of O_2 molecules during plasma discharge processes, electrons and UV and reactive species such as O, O^+, O^{2+}, O_2^+, and O_2^{2+} may be generated.[19] So, the O_2-plasma oxidation of MWCNTs not only introduces −C• free radicals but also leads to reaction with some of them, producing oxidized carbon species (C═O and O—C═O). The concentrations of the oxygen-containing groups may increase upon subsequent atmospheric exposure to air (O_2 and H_2O) because the $-C^{\bullet}$ free radical can react with O_2 and H_2O. In addition, it has been demonstrated that the presence of a defect site at the CNT surface results in an overall increase in the interaction strength such as binding energies and charge transfer between the tube and various molecules. So, the O_2 molecule lands on the CNTs and then dissociates barrierless into two O molecules, which subsequently bind on the defect site of the nanotube.[34] As a result, after O_2-plasma oxidation, oxygen-containing groups (C═O and O—C═O) are generated. Except for the above-mentioned reaction mechanisms, other reaction mechanisms might also have been in play during the plasma oxidation process because the active plasma particles may

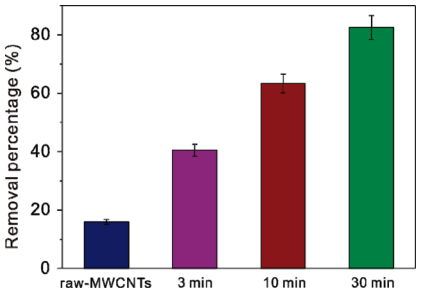

Figure 5. Effect of different plasma oxidation times on the adsorption of lead(II) onto MWCNTs (initial $C_{lead(II)}$ = 17 mg/L, pH = 5, m/V = 1.5 g/L, T = 293 K, and stirring time = 6 h).

induce radicals on different chemical bonds on the surfaces of the MWCNTs.[33] Here, we just took the radicals generated on the unsaturated bonds of sp^2 C═C as an example and illustrated the possible reactions on the surfaces of the MWCNTs.

Effect of the Plasma Oxidation Time on Adsorption. The dependences of lead(II) adsorption by the MWCNTs on the plasma oxidation time are presented in Figure 5. Compared with raw-MWCNTs, the plasma oxidation treatment had an evident impact on the adsorption capacity of MWCNTs for lead(II). The removal percentage of lead(II) increased after plasma oxidation. This can be attributed to the increase of the specific surface area, surface defects, and oxygen-containing functional groups, the removal of some caps of MWCNTs and amorphous carbon, and the improvement in dispersion in water after plasma oxidation. The mechanisms of metal-ion adsorption onto MWCNTs are very complicated and can be attributable to electrostatic attraction, adsorption−precipitation, and chemical interaction between the metal ions and the surface functional groups of MWCNTs.[32] However, it is commonly believed that the major sorption mechanism of heavy-metal ions onto carbon adsorbents is the chemical interaction between the heavy-metal ions and the surface functional groups of adsorbents and the improvement of adsorbability is mainly attributed to the change in the surface chemical structure rather than the surface physical structure.[7,13,32,35] In addition, it is noted that the amount of lead(II) adsorbed onto po-MWNCTs increased with the oxidation time. As demonstrated in the XPS measurement, the fraction of oxygen-containing functional groups increased with an increase of the plasma oxidation time. Thus, the MWCNTs oxidized for 30 min have the best adsorbability. In the following adsorption studies, the time of plasma oxidation was fixed at 30 min.

Adsorption Kinetics. Adsorption kinetics, which demonstrates the solute uptake rate, is one of the most important charactersistics. It represents the adsorption efficiency of adsorbents and therefore determines their potential applications. In order to better understand the dynamics of adsorption, the adsorption kinetics was investigated. The effect of the contact time on the removal of lead ions by raw-MWCNT and po-MWCNTs is depicted in Figure 6a. In both adsorbents, a rather fast adsorption of lead(II) occurred and then its equilibrium value was reached. The po-MWCNTs have higher adsorption capacity and faster adsorption efficiency toward lead(II) compared with raw-MWCNTs. The removal percentage of lead(II) was strongly dependent on the initial lead(II) concentrations. For raw-MWCNTs, the equilibrium was reached within 90 min for both concentrations of lead(II) used in this study, while for po-MWCNTs, the equilibrium was reached within 40 min. In the

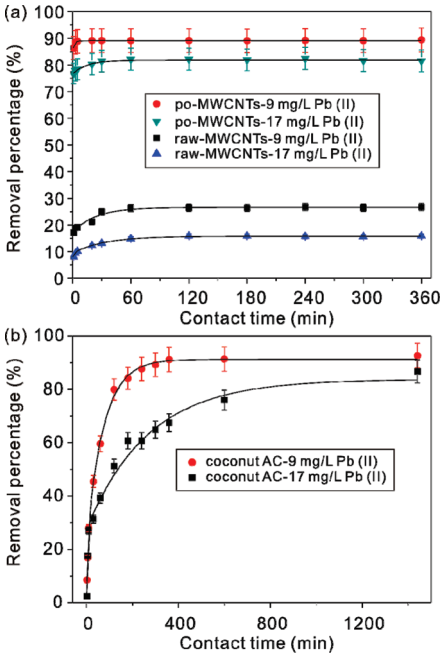

Figure 6. Effect of the contact time on the lead(II) absorption rate for different initial lead(II) concentrations onto (a) raw-/po-MWCNTs and (b) coconut shell AC (pH = 5.0, m/V = 1.5 g/L, and T = 293 K).

following adsorption studies, a contact time of 3 h was selected for the rest of the batch experiments to make sure that equilibria were reached for adsorption of lead(II) onto MWCNTs. Figure 6b shows the effect of the contact time on lead(II) absorption for different initial lead(II) concentrations onto coconut shell AC. Obviously, it can be seen that it took above 6 and 12 h to reach equilibrium at lead(II) concentrations of 9 and 17 mg/L onto coconut shell AC, respectively.

To investigate the adsorption kinetics of lead(II) with these adsorbents, two kinetic models (pseudo-first-order and pseudo-second-order) were tested against the experimental data. The pseudo-first-order and pseudo-second-order models are presented as follows:[8,10]

$$log(q_e - q_t) = log\ q_e - \frac{k_1}{2.303}t \quad (2)$$

$$\frac{t}{q_t} = \frac{1}{k_2 q_e^2} + \frac{1}{q_e}t \quad (3)$$

where q_e and q_t are the amounts of lead(II) adsorbed at equilibrium and at time t, respectively. k_1 is the rate constant of the pseudo-first-order adsorption process $(1/min)$[8,10] and k_2 is the rate constant of the pseudo-second-order model of adsorption (g/mg/min).[2,8,10] For the pseudo-first-order model, the values of k_1 and q_e were calculated from the slope and intercept of plots of $\log(q_e - q_t)$ versus t. For the pseudo-second-order model, the values of k_2 and q_e can be obtained by a plot of t/q_t against t. Because the correlation coefficient values for the pseudo-first-order model are all below 0.85, the kinetic parameters and the fitting curves of the pseudo-first-order model are not shown here. The pseudo-second-order kinetic plots for the adsorption of lead(II) onto MWCNTs and coconut shell AC are shown in parts a and b of Figure 7, respectively. The correlation coefficient values for the pseudo-second-order model are all

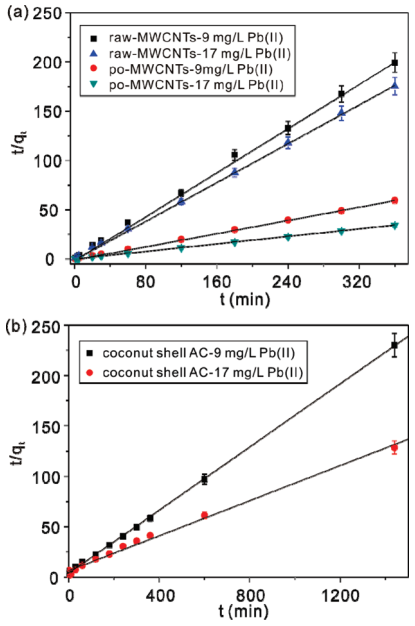

Figure 7. Pseudo-second-order kinetic plots for the adsorption of lead(II) onto (a) raw-/po-MWCNTs and (b) coconut shell AC.

above 0.99 (Table S3 in the Supporting Information), suggesting that the pseudo-second-order model best represents the adsorption kinetics in our adsorbent systems. Moreover, from Table S3 in the Supporting Information, we can see that the q values ($q_{e,cal}$) calculated from the pseudo-second-order model are consistent with the experimental q values ($q_{e,exp}$). Table S3 in the Supporting Information also shows the kinetic parameters for adsorption of lead(II) by raw-MWCNTs, po-MWCNTs, and coconut shell AC. The adsorption capacity of po-MWCNTs is comparable to coconut shell AC; however, the time to reach equilibrium for lead(II) adsorption onto po-MWCNTs was much shorter than that onto coconut shell AC. In other words, po-MWCNTs have higher adsorption efficiencies than that of coconut shell AC. Because the adsorption efficiency is one of the considerations for potential water purification plant applications, the po-MWCNTs are more suitable for a continuous-flow system.

Effect of the pH on Adsorption. The pH is one of the most important factors that affect the hydrolysis, complexation, and precipitation of lead(II) and the sites of dissociation of MWCNTs.[10] In this study, the adsorption experiments have been conducted in the initial pH range of 2.0−9.0. The results are shown in Figure 8. The adsorption performances of lead(II) onto raw-MWCNTs have also been shown for comparison purposes. The removal of lead(II) by raw-MWCNTs and po-MWCNTs was highly dependent on the pH value. It is obvious that, at any pH value, the adsorption percentage of lead(II) onto po-MWCNTs was higher than that onto raw-MWCNTs. With increasing pH values, the adsorption percentage first increased and then changed negligibly for both adsorbents. The pH is a significant factor for determining the existing form of the metallic species in aqueous solution. It is known that lead species are mainly present in the forms of Pb^{2+}, $Pb(OH)^+$, and $Pb(OH)_2$ at pH < 9.[14,36] At pH < 6, the predominant lead species is Pb^{2+}, and the removal of Pb^{2+} was mainly attributed to the adsorption reaction. Pb^{2+} adsorption that took place at low pH can be attributed mainly to the competition between H^+ and Pb^{2+} ions on the surface sites.[14,36] At pH = 6−7, the main lead species are

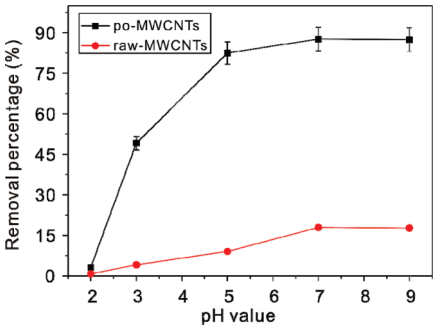

Figure 8. Effect of the pH on lead(II) adsorption onto raw-MWCNTs and po-MWCNTs (initial $C_{lead(II)}$ = 17 mg/L, m/V = 1.5 g/L, and T = 293 K).

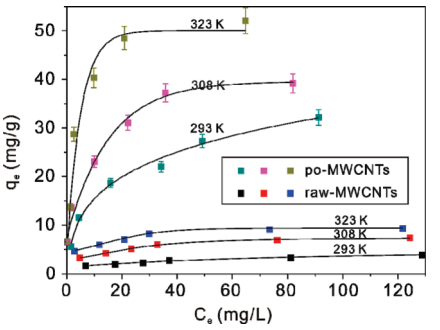

Figure 9. Lead(II) adsorption isotherms onto raw-MWCNTs and po-MWCNTs at various temperatures (pH = 5.0 and m/V = 1.5 g/L).

Pb^{2+} and $Pb(OH)^+$, and the electrostatic attraction between the negatively charged MWCNT surface and the positively charged Pb^{2+} and $Pb(OH)^+$ may be responsible for the removal of lead(II).[2,36] In the case of high pH values (7−9), the removal of lead remained constant and reached a maximum. Because the main species at pH = 7−9 are Pb^{2+}, $Pb(OH)^+$, and $Pb(OH)_2$, the removal of lead was possibly accomplished by the simultaneous precipitation of $Pb(OH)_2$ and the adsorption of Pb^{2+} and $Pb(OH)^+$.[14,36]

Adsorption Isotherms. Figure 9 shows the adsorption isotherms of lead(II) on raw-MWCNTs and po-MWCNTs at 293, 308, and 323 K. Two empirical equations, the Langmuir and Freundlich isotherm models, were used to analyze the experimental data. The Langmuir isotherm assumes a surface with homogeneous binding sites, equivalent adsorption energies, and no interaction between adsorbed species. Therefore, the adsorption saturates and no further adsorption occurs. Meanwhile, the Freundlich isotherm is based on an exponential distribution of adsorption sites and energies. It is derived to model multilayer adsorption and adsorption onto heterogeneous surfaces. The mathematical expressions of the Langmuir and Freundlich isotherm models are[37,38]

$$\frac{C_e}{q_e} = \frac{1}{q_m K_L} + \frac{C_e}{q_m} \quad (4)$$

$$ln\ q_e = \frac{1}{n} ln\ C_e + ln\ K_F \quad (5)$$

where q_m and K_L are Langmuir constants representing the maximum adsorption capacity of adsorbents (mg/g) and the

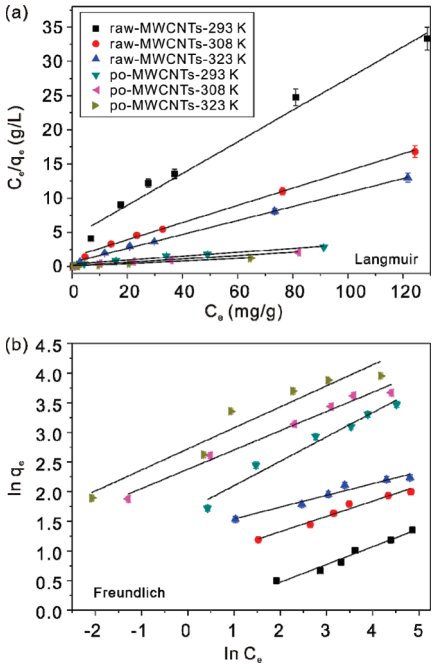

Figure 10. Linearized (a) Langmuir and (b) Freundlich isotherms for lead(II) adsorption by raw-MWCNTs and po-MWCNTs at various temperatures.

energy of adsorption, respectively. K_F and n are Freundlich constants related to the adsorption capacity and adsorption intensity, respectively.

For the Langmuir isotherm model, the values of q_m and K_L can be calculated from the slope and intercept of plots of C_e/q_e versus C_e. For the Freundlich isotherm model, the values of n and K_F can be obtained by a plot of $\ln q_e$ against $\ln C_e$. The parameters of the Langmuir and Freundlich models were calculated (Table S4 in the Supporting Information), and the curve-fitting results are shown in Figure 10a,b. From the correlation coefficients, it can be seen that the adsorption data fit the Langmuir isotherm model better than the Freundlich isotherm model. From Table S4 in the Supporting Information, the maximum adsorption capacity q_m increases with the temperature for both raw-MWCNTs and po-MWCNTs. At the same temperature, q_m of lead(II) with po-MWCNTs is much higher than that with raw-MWCNTs, which illustrates that the adsorption capacity of MWCNTs for lead(II) can be enhanced with O_2-plasma oxidation. In addition, the values of K_L for po-MWCNTs are larger than those for raw-MWCNTs at the same temperature, suggesting that po-MWCNTs have a higher affinity for lead(II) than raw-MWCNTs.[38] Optimization of the operation parameters of plasma oxidation such as the plasma power and gas pressure is ongoing in order to introduce more oxygen-containing functional groups onto MWCNTs without changing their bulk properties.

Adsorption Thermodynamics. Because the thermodynamic parameters are actually helpful in the practical application of the process, adsorption thermodynamics were studied. The lead(II) adsorption capacity increases with an increase of the temperature, indicating that the adsorption of lead(II) onto MWCNTs is an endothermic reaction. This can be explained by the fact that the increase of the temperature results in a rise in the diffusion rate of metal ions across the boundary layers and within the pores of MWCNTs because of decreasing solution viscosity.[32]

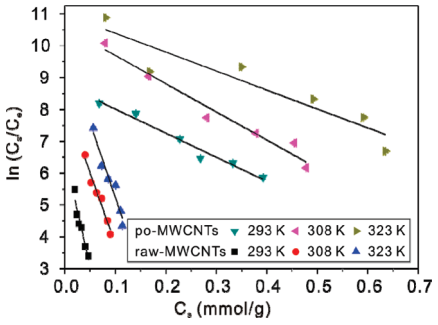

Figure 11. Plots of $\ln C_S/C_e$ as a function of C_S for raw-MWCNTs and po-MWCNTs at various temperatures.

Thermodynamic parameters were calculated from variation of the thermodynamic equilibrium constant K_0 with a change in the temperature. K_0 is defined as follows:[1,2]

$$K_0 = \frac{a_S}{a_e} = \frac{\nu_S}{\nu_e}\frac{C_S}{C_e} \quad (6)$$

where a_S is the activity of adsorbed lead(II), a_e is the activity of lead(II) in solution at equilibrium, ν_S is the activity coefficient of adsorbed lead(II), ν_e is the activity coefficient of lead(II) in solution, C_S is the amount of lead(II) adsorbed by per mass of MWCNTs (mmol/g), and C_e is the concentration of lead(II) in solution at equilibrium (mmol/mL).

As the lead(II) concentration in the solution decreases and approaches zero, K_0 can be calculated by plotting $\ln(C_S/C_e)$ versus C_S (Figure 11) and extrapolating C_S to zero. The values of K_0 can be obtained from the intercept of the plot. The Gibbs energy (ΔG°) of adsorption is calculated from the equation[1,2]

$$\Delta G^\circ = -RT \ln K_0 \quad (7)$$

where R is the ideal gas constant (8.3145 J/mol/K) and T (K) is the absolute temperature.

The average change of the standard enthalpy ΔH° is obtained from the van't Hoff equation:

$$\ln K_0(T_3) - \ln K_0(T_1) = \frac{-\Delta H^\circ}{R}\left(\frac{1}{T_3} - \frac{1}{T_1}\right) \quad (8)$$

where T_3 and T_1 are two different temperatures. The standard entropy change

$$\Delta S^\circ = -\frac{\Delta G^\circ - \Delta H^\circ}{T} \quad (9)$$

The calculated values of thermodynamic parameters are listed in Table S5 in the Supporting Information. The negative Gibbs free-energy values (ΔG°) confirm that adsorption is spontaneous under ambient conditions.[1,2,32] The values of ΔG° at higher temperature are more negative than those at lower temperature, indicating the more efficient adsorption at higher temperature. The positive values of ΔH° for lead(II) suggest an endothermic nature of adsorption. The positive values for ΔS° may be due to the release of water molecules produced by an ion-exchange reaction between the metal ions and the surface functional groups of MWCNTs, reflecting the affinity of MWCNTs for Pb^{2+} ions and an increase in the randomness at the solid−solution interface during the adsorption process.[1,32]

Proposed Removal Mechanism. In order to investigate the existing form of lead(II) on po-MWCNTs and the interaction

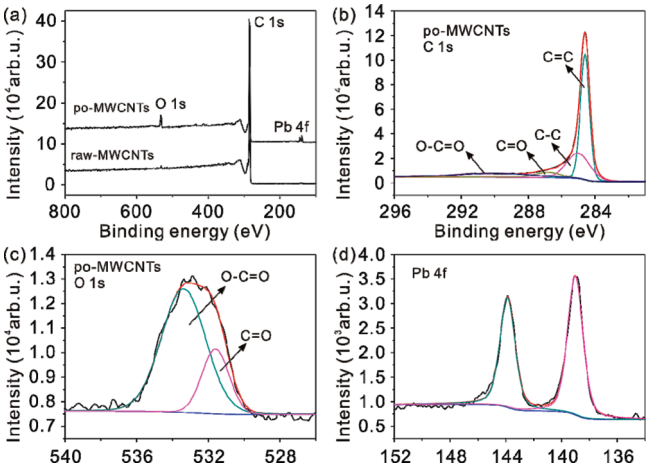

Figure 12. (a) XPS wide scan of raw-MWCNTs and po-MWCNTs after adsorption of lead(II). (b and c) High resolution of C 1s and O 1s spectra of po-MWCNTs, respectively. (d) High resolution of the Pb 4f spectrum of po-MWCNTs.

between lead(II) and oxygen-containing functional groups, XPS of raw-MWCNTs and po-MWCNTs and C 1s, O 1s, and Pb 4f high-resolution XPS data of po-MWCNTs after lead(II) adsorption (pH = 5, initial $C_{lead(II)}$ = 134 mg/L, and T = 293 K) are shown in Figure 12. Compared with raw-MWCNTs, there are two obvious peaks of Pb 4f in the wide-scan spectra of po-MWCNTs (Figure 12a). The high-resolution C 1s spectra of po-MWCNTs change little before and after lead(II) adsorption and can also be resolved into four individual component peaks located at 284.6, 285.0, 286.8, and 289.9 eV, which represent graphitelike sp^2 carbon, diamondlike sp^3 carbon, and carbon in carbonyl (or ether) groups and carboxyl (or ester) groups, respectively (Figure 12b). The high-resolution O 1s spectra of po-MWCNTs after adsorption of lead(II) have been resolved into two individual component peaks located at 531.6 and 533.4 eV, which can be assigned to the oxygen atoms in the C═O (531.6 eV) groups and O−C═O (533.4 eV) groups, respectively (Figure 12c). The high-resolution Pb 4f spectrum can be fitted to two peaks, which appear at 139.0 eV (assigned to Pb $4f_{7/2}$) and at 143.9 eV (assigned to Pb $4f_{5/2}$), respectively (Figure 12d). The Pb $4f_{7/2}$ peak at about 139.0 eV can be attributed to $(MWCNT-COO)_2Pb$ and $MWCNT-COOPb^+$, which were formed through the reaction of Pb^{2+} with functional groups on the surface of po-MWCNTs.[13,14] So, the lead(II) adsorbed onto the surfaces of po-MWCNTs is mainly in the form of $(MWCNT-COO)_2Pb$ and $MWCNT-COOPb^+$. The possible adsorption reactions may be as follows:

$$(MWCNT-COOH)_2 + Pb^{2+} \rightarrow (MWCNT-COO)_2Pb + 2H^+ \quad (10)$$

$$MWCNT-COOH + Pb^{2+} \rightarrow MWCNT-COOPb^+ + H^+ \quad (11)$$

It is worth saying that the above adsorption reactions are not the only reactions of lead(II) with MWCNTs; however, the complex and ion-exchange reactions between MWCNT−COOH and Pb^{2+} are the chief adsorption reactions in this study.

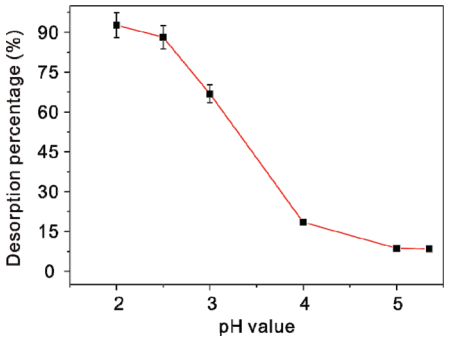

Figure 13. Desorption of lead(II) from po-MWCNTs by adjustment of the pH of the solution (m/V = 1.5 g/L and T = 293 K).

Desorption Study. Reversibility, which decides the cost of adsorption to some extent, is very important for the practical application of an adsorbent. An advanced adsorbent should possess both higher adsorption capacity and better desorption property. Figure 13 shows the lead(II) desorption percentages with regard to solutions at various pH values. It is apparent that the lead(II) desorption percentage increased with a decrease of the pH value of the solution. The percentage of desorption increased sharply at pH = 4.0 and eventually reached about 93% at pH = 2.0. The above results show that the lead(II) adsorbed by po-MWCNTs can be easily desorbed and the po-MWCNTs can be employed repeatedly in heavy-metal water purification. Furthermore, the regeneration process also indicates that ion exchange is one of the main adsorption mechanisms.

4. CONCLUSIONS

We have developed a mild surface functionalization process to oxidize MWCNTs for the adsorption of lead(II) in drinking water. Compared with the acid oxidation method, the O_2-plasma-oxidation technique is a time-efficient and environmentally friendly method. The bulk structure of MWCNTs was not destroyed after O_2-plasma oxidation. In addition, the specific surface area of MWCNTs was increased and oxygen-containing functional groups were successfully grafted onto MWCNTs. The O_2-plasma-oxidized MWCNTs were easily dispersed in water. The adsorption capacity of MWCNTs was greatly enhanced after O_2-plasma oxidation, which was mainly due to the introduction of oxygen-containing functional groups. The adsorption capacity of plasma-oxidized MWCNTs for lead(II) is comparable to that of coconut shell AC; however, the kinetic properties of plasma-oxidized MWCNTs are far better than those of coconut shell AC. The kinetic adsorption process can be well described by the pseudo-second-order model for the adsorbents in this study. The removal of lead(II) by MWCNTs is highly dependent on the pH value. The thermodynamic parameters indicate that the interaction of lead(II) adsorbed by MWCNTs is endothermic and spontaneous. The predominant mechanism for lead(II) adsorbed onto O_2-plasma-oxidized MWCNTs is the reaction of lead(II) with functional groups on the surface of po-MWCNTs. Lead(II) can be easily desorbed from plasma-oxidized MWCNTs by adjusting the solution pH values; thus, the O_2-plasma-oxidized MWCNTs exhibit promising application potentials as an adsorbent in water purification.

■ ASSOCIATED CONTENT

Supporting Information. Possible mechanism of MWCNTs oxidized by O_2 plasma, the specific surface area and pore

structure parameters of raw-MWCNTs and po-MWCNTs, the results of XPS and Raman spectroscopy of raw-MWCNTs and po-MWCNTs oxidized with different plasma oxidation times, pseudo-second-order kinetic parameters for the adsorption of lead(II) onto raw-MWCNTs, po-MWCNTs, and coconut shell AC at various initial lead(II) concentrations, parameters of the Langmuir and Freundlich models for adsorption of lead(II) onto raw-MWCNTs and po-MWCNTs at various temperatures, and thermodynamic parameters for lead(II) adsorption onto raw-MWCNTs and po-MWCNTs. This material is available free of charge via the Internet at http://pubs.acs.org.

AUTHOR INFORMATION

Corresponding Author

*E-mail: xingjiuhuang@iim.ac.cn (X.-J.H), jhliu@iim.ac.cn (J.-H.L). Tel.: +86-551-5591142. Fax: +86-551-5592420.

ACKNOWLEDGMENT

This work was supported by the One Hundred Person Project of the Chinese Academy of Sciences, China, the National Key Scientific Program, Nanoscience and Nanotechnology (Grant 2011CB933700), and the National Natural Science Foundation of China (Grants 60801021 and 20907035).

REFERENCES

(1) Li, Y.; Di, Z.; Ding, J.; Wu, D.; Luan, Z.; Zhu, Y. *Water Res.* **2005**, *39*, 605.
(2) Wang, S.; Gong, W.; Liu, X.; Yao, Y.; Gao, B.; Yue, Q. *Sep. Purif. Technol.* **2007**, *58*, 17.
(3) Zhang, S.; Shao, T.; Bekaroglu, S. S. K.; Karanfil, T. *Water Res.* **2010**, *44*, 2067.
(4) Yang, K.; Xing, B. *Environ. Pollut.* **2009**, *157*, 1095.
(5) Liao, Q.; Sun, J.; Gao, L. *Carbon* **2008**, *46*, 553.
(6) Chen, G.-C.; Shan, X.-Q.; Wang, Y.-S.; Wen, B.; Pei, Z.-G.; Xie, Y.-N.; Liu, T.; Pignatello, J. J. *Water Res.* **2009**, *43*, 2409.
(7) Cho, H.-H.; Wepasnick, K.; Smith, B. A.; Bangash, F. K.; Fairbrother, D. H.; Ball, W. P. *Langmuir* **2010**, *26*, 967.
(8) Hu, J.; Chen, C.; Zhu, X.; Wang, X. *J. Hazard. Mater.* **2009**, *162*, 1542.
(9) Kabbashi, N. A.; Atieh, M. A.; Al-Mamun, A.; Mirghami, M. E. S.; Alam, M. D. Z.; Yahya, N. *J. Environ. Sci.* **2009**, *21*, 539.
(10) Kuo, C.-Y.; Lin, H.-Y. *Desalination* **2009**, *249*, 792.
(11) Li, Y.; Zhu, Y.; Zhao, Y.; Wu, D.; Luan, Z. *Diamond Relat. Mater.* **2006**, *15*, 90.
(12) Wang, H.; Zhou, A.; Peng, F.; Yu, H.; Chen, L. *Mater. Sci. Eng., A* **2007**, *466*, 201.
(13) Wang, H.; Zhou, A.; Peng, F.; Yu, H.; Yang, J. *J. Colloid Interface Sci.* **2007**, *316*, 277.
(14) Xu, D.; Tan, X.; Chen, C.; Wang, X. *J. Hazard. Mater.* **2008**, *154*, 407.
(15) Li, Y.; Wang, S.; Wei, J.; Zhang, X.; Xu, C.; Luan, Z.; Wu, D.; Wei, B. *Chem. Phys. Lett.* **2002**, *357*, 263.
(16) Tseng, W.-S.; Tseng, C.-Y.; Chuang, P.-K.; Lo, A.-Y.; Kuo, C.-T. *J. Phys. Chem. B* **2008**, *112*, 18431.
(17) Jiang, Z.; Yu, X.; Jiang, Z.-j.; Meng, Y.; Shi, Y. *J. Mater. Chem.* **2009**, *19*, 6720.
(18) Felten, A.; Bittencourt, C.; Pireaux, J. J.; Van Lier, G.; Charlier, J. C. *J. Appl. Phys.* **2005**, *98*, 074308.
(19) Naseh, M. V.; Khodadadi, A. A.; Mortazavi, Y.; Pourfayaz, F.; Alizadeh, O.; Maghrebi, M. *Carbon* **2010**, *48*, 1369.
(20) Xu, T.; Yang, J.; Liu, J.; Fu, Q. *Appl. Surf. Sci.* **2007**, *253*, 8945.
(21) Charlier, J.-C.; Arnaud, L.; Avilov, I. V.; Delgado, M.; Demoisson, F.; Espinosa, E. H.; Ewels, C. P.; Felten, A.; Guillot, J.; Ionescu, R.; Leghrib, R.; Llobet, E.; Mansour, A.; Migeon, H.-N.; Pireaux, J.-J.; Reniers, F.; Suarez-Martinez, I.; Watson, G. E.; Zanolli, Z. *Nanotechnology* **2009**, *20*, 375501.
(22) Zanolli, Z.; Leghrib, R.; Felten, A.; Pireaux, J.-J.; Llobet, E.; Charlier, J.-C. *ACS Nano* **2011**, DOI: 10.1021/nn200294h.
(23) Lippens, B. C.; de Boer, J. H. *J. Catal.* **1965**, *4*, 319.
(24) Lastoskie, C.; Gubbins, K. E.; Quirke, N. *J. Phys. Chem.* **1993**, *97*, 4786.
(25) Zhang, X.; Lei, L.; Xia, B.; Zhang, Y.; Fu, J. *Electrochim. Acta* **2009**, *54*, 2810.
(26) Zhang, H.; Guo, H.; Deng, X.; Gu, P.; Chen, Z.; Jiao, Z. *Nanotechnology* **2010**, *21*, 085706.
(27) Jahagirdar, C. J.; Srivastava, Y. *J. Appl. Polym. Sci.* **2001**, *82*, 292.
(28) Dresselhaus, M.; Dresselhaus, G.; Saito, R.; Jorio, A. *Phys. Rep.* **2005**, *409*, 47.
(29) Osswald, S.; Havel, M.; Gogotsi, Y. *J. Raman Spectrosc.* **2007**, *38*, 728.
(30) Yoo, K.-P.; Kwon, K.-H.; Min, N.-K.; Lee, M. J.; Lee, C. J. *Sens. Actuators, B* **2009**, *143*, 333.
(31) Kodama, S.; Habaki, H.; Sekiguchi, H.; Kawasaki, J. *Thin Solid Films* **2002**, *407*, 151.
(32) Rao, G.; Lu, C.; Su, F. *Sep. Purif. Technol.* **2007**, *58*, 224.
(33) Tang, S.; Lu, N.; Wang, J. K.; Ryu, S.-K.; Choi, H.-S. *J. Phys. Chem. C* **2007**, *111*, 1820.
(34) Zanolli, Z.; Charlier, J.-C. *Phys. Rev. B* **2009**, *80*, 155447.
(35) Lee, D.; Hong, S.; Paek, K.; Ju, W. *Surf. Coat. Technol.* **2005**, *200*, 2277.
(36) Gupta, V. K.; Agarwal, S.; Saleh, T. A. *J. Hazard. Mater.* **2011**, *185*, 17.
(37) Zhang, X.; Jia, Q.; Song, N.; Zhou, W.; Li, Y. *J. Chem. Eng. Data* **2010**, *55*, 4428.
(38) Li, Y.; Liu, F.; Xia, B.; Du, Q.; Zhang, P.; Wang, D.; Wang, Z.; Xia, Y. *J. Hazard. Mater.* **2010**, *177*, 876.